ECCOMAS Congress 2016
VII European Congress on Computational Methods in Applied Sciences and Engineering
M. Papadrakakis, V. Papadopoulos, G. Stefanou, V. Plevris (eds.)
Crete Island, Greece, 5–10 June 2016

BUDGET ANALYSIS OF TURBULENT KINETIC ENERGY IN CORNER SEPARATION : RANS VS LES

Jean-François Monier[1,3], Feng Gao[2], Jérôme Boudet[1], Liang Shao[1], Lipeng Lu[4]

[1]Univ Lyon, École Centrale de Lyon, Laboratoire de Mécanique des Fluides et d'Acoustique,
UMR CNRS 5509, 36, avenue Guy de Collongue F-69134, Écully cedex, France
e-mail: jean-francois.monier@doctorant.ec-lyon.fr, jerome.boudet@ec-lyon.fr, liang.shao@ec-lyon.fr

[2]University of Surrey
Guildford, Surrey GU2 7XH, United Kingdom
e-mail: f.gao@surrey.ac.uk

[3]SNECMA
Rond-point René Ravaud, 77550 Moissy-Cramayel
e-mail: jean-francois.monier@doctorant.ec-lyon.fr

[4]Beihang University
37 Xueyuan Road, Haidian District, Beijing 100191, China
e-mail: lulp@buaa.edu.cn

Keywords: Linear compressor cascade, Corner separation, Large-eddy simulation, Reynolds-averaged Navier-Stokes, Reynolds stresses, Turbulent kinetic energy budget

Abstract. *The aim of the study is to compare the LES of corner separation, considered as a reference, in the LMFA-NACA65 linear compressor cascade to RANS simulations using Wilcox two-equation models ($k-\omega$). The LES was carried-out by Gao et al. [1] using the Shear-improved Smagorinsky model (SISM), and has been validated by comparison with the experimental data obtained by Ma et al. [2]. Two steady RANS simulations are carried out using $k-\omega$ models: Wilcox 1988 model and Wilcox 1988 model with quadratic constitutive relation.*

First, the analysis will consider the total pressure losses on a two-dimensional section downstream of the cascade. The Reynolds stresses and the turbulent kinetic energy budget are analysed within the separation region, on a two-dimensional section at the trailing edge of the blade. The RANS simulations mostly overestimate the total pressure losses and the size of the corner separation, compared to the LES and the experiment. The RANS simulations also overestimate the level of the Reynolds stresses and the terms of the turbulent kinetic energy budget, compared to the LES. The quadratic constitutive relation yields some modifications, but not significant enough to have results comparable to LES.

1 INTRODUCTION

The economical and environmental cost reduction in jet engines is linked with the capacity to reduce their size and mass, i.e. increasing the pressure ratio. This leads to an increase of the blade loading, which is known to worsening the three-dimensional flow phenomena. One of those phenomena is the corner separation, i.e. the separation occurring when two orthogonal boundary-layers interact. For a compressor it occurs at the junction of the end-wall and the blade suction side. The corner separation has been investigated experimentally on linear compressor cascades [3, 4, 2, 5], and numerically [6], but its physics is not yet entirely understood.

Numerical simulations give access to a lot of information on the flow behaviour, and are widely used for turbo-machinery development. Reynolds-averaged Navier-Stokes (RANS) simulations are commonly used by industries. In the case of corner separation, RANS simulations tend to over-predict its size and intensity [7, 8, 9]. Bordji *et al.* [10] found that using a non-Boussinesq constitutive relation (the quadratic constitutive relation, referred to as QCR [11]) yields better results for external flows. Large-eddy simulation (LES) is able to simulate three-dimensional secondary flows [12] and is better at simulating corner separation [1, 13] but at a much greater computational cost, which keep industries from using it for conception.

The turbulence physics simulated by both RANS and LES (validated against experimental results) are investigated in order to understand why RANS simulations fail to predict correctly the corner separation characteristics. Reynolds stresses and turbulent kinetic energy budgets from LES and RANS with both original Wilcox $k-\omega$ model and QCR version are compared at the trailing edge of the blade.

2 EXPERIMENTAL SET-UP

Ma *et al.* [2, 5] lead an experimental campaign on the LMFA-NACA65 linear cascade. The sketch of the experimental set-up is given figure 1. The blade has a chord $c = 150.0$mm, a stagger angle $\gamma = 42.7°$, a pitch $s = 134.0$mm and a span $h = 370.0$mm. Inlet velocity is set to 40m/s, which gives a chord-based Reynolds number of 3.82×10^5. Experimental results used in this paper were acquired for an incidence angle $i = 4°$, where a corner separation has been found. More information concerning the experiment can be found in Ref.[2, 5, 14].

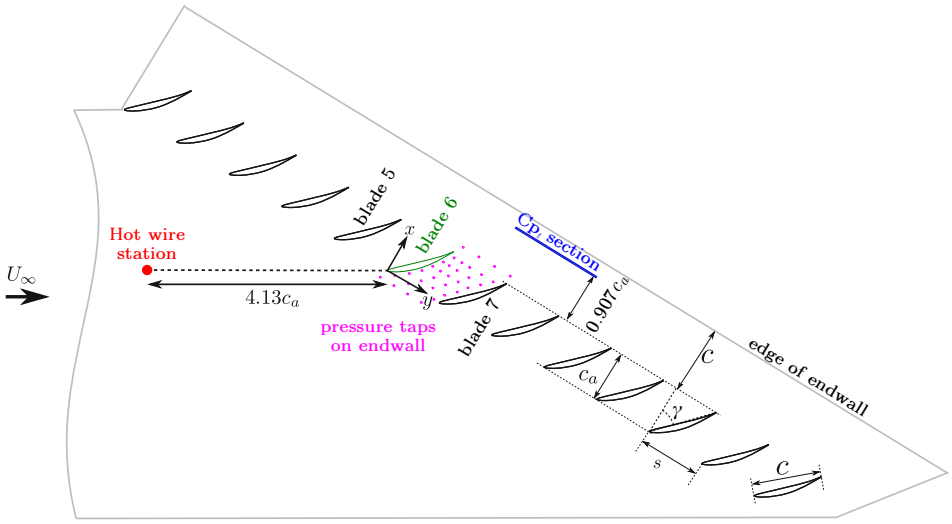

Figure 1: Sketch of the LMFA-NACA65 experimental set-up

3 NUMERICAL METHODS

3.1 Notations

In order to avoid any ambiguity on the notations, the symbols denoting the ensemble average and the low frequency filter are kept in the equations. The ensemble average of a quantity φ is noted $\langle\varphi\rangle$, the Favre ensemble average is noted $[\varphi]$ ($[\varphi] = \langle\rho\varphi\rangle \,/\, \langle\rho\rangle$), the low frequency filter is noted $\overline{\varphi}$ and the Favre low frequency filter is noted $\widetilde{\varphi}$ ($\widetilde{\varphi} = \overline{\rho\varphi}/\overline{\rho}$). Moreover, the fluctuating part of the low-frequency filtered quantity is noted φ' (thus, $\overline{\varphi} = \langle\overline{\varphi}\rangle + \varphi'$) and the Favre fluctuating part of the Favre low frequency filtered quantity is noted φ'' (thus, $\widetilde{\varphi} = [\widetilde{\varphi}] + \varphi''$).

The coordinate system used is the same as in the experiment (Fig. 1). By convention, x and x_1 both represent the stream-wise direction, y and x_2 both represent the pitch-wise direction and z and x_3 both represent the span-wise direction. Consequently, u and u_1 both represent the stream-wise velocity, v and u_2 both represent the pitch-wise velocity and w and u_3 both represent the span-wise velocity.

3.2 General specifications

The numerical simulations have been carried out with the solver *Turb'Flow*, a compressible code developed at LMFA relying on finite volume discretization. *Turb'Flow* specifications are given in Ref.[15].

3.3 Large-Eddy Simulation

The LES, done by Gao [1], uses a mesh well defined close to the walls ($\simeq 200 \times 10^6$ points, $y^+ \simeq 1$). The spatial scheme is a 4-point Jameson centered scheme [16] with an artificial viscosity coefficient of 0.002 [17]. The temporal scheme is a 3-step Runge-Kutta scheme with a constant time step of 2.5×10^{-8}s, corresponding to a CFL (Courant-Friedrichs-Lewy condition) number close to 0.95. The LES relies on the SISM (shear-improved Smagorinsky model) subgrid scale model of Lévêque *et al.* [18]:

$$\mu_{SGS} = \overline{\rho}\,(C_s\Delta)^2\left(\left|\widetilde{\mathbf{S}}\right| - \left|\left\langle\widetilde{\mathbf{S}}\right\rangle\right|\right), \text{ with } \left|\widetilde{\mathbf{S}}\right| = \left(2\widetilde{S}_{ij}\widetilde{S}_{ij}\right)^{1/2} \text{ and } C_s = 0.18 \qquad (1)$$

where μ_{SGS} is the sub-grid scale viscosity, $\overline{\rho}$ is the density, C_s is the constant of the original Smagorinsky model, Δ is a measure of the grid spacing (practically, the cubic root of the grid cell volume) and $\widetilde{\mathbf{S}}$ is the low frequency strain rate tensor. The average $\langle\ \rangle$ is estimated with an exponential smoothing [19], with a cut-off frequency of 533 Hz based on the ratio between twice the free-stream velocity and the chord. Complete details of the LES specifications are given in Ref. [1].

The Reynolds stresses extracted from the LES results are defined as follow:

$$\boldsymbol{\tau}_{\mathbf{t}} = -\left\langle\overline{\rho}\mathbf{u}'' \otimes \mathbf{u}''\right\rangle \qquad (2)$$

A Reynolds stress budget can be extracted, following the method of Gao [20]. The turbulent kinetic energy budget (referred to as TKE budget) is then deduced from the Reynolds stress budget diagonal terms addition ($k = \frac{1}{2}u_i''u_i''$). Theoretically, the TKE budget is balanced. However, there is practically a residual, with a dissipative effect. This residual represents the various numerical dissipations, such as numerical scheme dissipation. A term of numerical dissipation, noted Ξ and calculated as the opposite of the residual, is added in the budget to close it.

$$\frac{\partial \langle \overline{\rho} k \rangle}{\partial t} = 0 = \underbrace{-\frac{\partial}{\partial x_j}\left(\langle \overline{\rho} k \rangle \left[\widetilde{u_j}\right]\right)}_{\text{Advection}} \underbrace{-\left\langle \overline{\rho} u_i'' u_j'' \right\rangle \frac{\partial \left[\widetilde{u_i}\right]}{\partial x_j}}_{\text{Production}} \underbrace{-\frac{\partial}{\partial x_j}\left(\left\langle \overline{\rho} k u_j'' \right\rangle\right)}_{\text{Turbulent diffusion}} \underbrace{-\frac{\partial \left\langle u_i'' p' \right\rangle}{\partial x_i}}_{\text{Pressure diffusion}} \underbrace{+\left\langle p' \frac{\partial u_i''}{\partial x_i} \right\rangle}_{\text{Pressure dilatation}}$$
$$\underbrace{-\left\langle u_i'' \right\rangle \frac{\partial \langle \overline{p} \rangle}{\partial x_i}}_{} \underbrace{+\frac{\partial \left\langle \overline{\tau_{ij}} u_i'' \right\rangle}{\partial x_j}}_{\text{Viscous diffusion}} \underbrace{-\left\langle \overline{\tau_{ij}} \frac{\partial u_i''}{\partial x_j} \right\rangle}_{\text{Viscous dissipation}} \underbrace{+\frac{\partial \left\langle \overline{\Pi_{ij}} u_i'' \right\rangle}{\partial x_j}}_{\text{SGS diffusion}} \underbrace{-\left\langle \overline{\Pi_{ij}} \frac{\partial u_i''}{\partial x_j} \right\rangle}_{\text{SGS Dissipation}} \underbrace{+\Xi_{ii}}_{\text{Numerical dissipation}} \quad (3)$$

The LES TKE budget, presented in equation (3), shows more terms than the RANS equation of k. In order to compare these two, some terms are grouped. Production and numerical dissipation are kept apart. The dissipation term is the sum of the viscous dissipation and the SGS dissipation. All the other terms are summed to form the transport term.

3.4 Reynolds-Averaged Navier-Stokes

The RANS simulations use the reference mesh from Gao [20] for the incidence $i = 4°$. This mesh is a coarser version of the LES mesh ($\simeq 2.8 \times 10^6$ points) with no trip bands (cf. Fig. 2). The spatial scheme is a 4-point Jameson centered spatial scheme with an artificial viscosity coefficient of 0.02. The temporal scheme is a 5-step Runge-Kutta scheme with a CFL number of 0.7. Two turbulence models are investigated, the original Wilcox $k-\omega$ model [21] and a modified version using the QCR from Spalart [11]. The inlet conditions (density, velocity and turbulent variables) are extracted from a 2-D flat plate boundary layer simulation at the position where momentum boundary layer thickness δ_1 matches the experiment. The outlet is set to a partially non reflective pressure condition. The walls boundary conditions are set to non-slip adiabatic. The lateral boundary conditions are set to periodic. The mid-span boundary condition is set to symmetry, given that only half the channel is simulated.

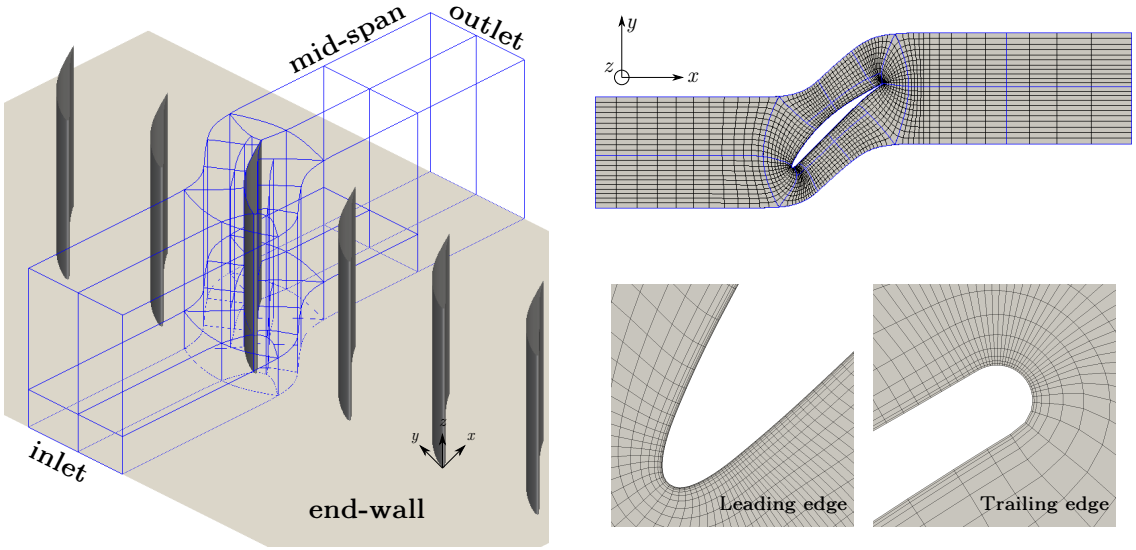

(a) View of the computational domain

(b) View of the blade-to-blade mesh

Figure 2: Views of the computational domain and the mesh. The mesh is coarsened in order to be displayed.

The original Wilcox $k-\omega$ model [21] calculates the Reynolds stress tensor $\boldsymbol{\tau_t}$ using Boussinesq constitutive relation:

$$\tau_{t,ij} = 2\mu_t S_{ij}^{(0)} - \frac{2}{3}\delta_{ij}\left\langle\rho\right\rangle[k] \text{ , where } \mu_t = \left\langle\rho\right\rangle\frac{[k]}{[\omega]} \tag{4}$$

with δ_{ij} the Kroeneker symbol and $S^{(0)}$ the zero-trace strain rate tensor:

$$S_{ij}^{(0)} = S_{ij} - \frac{1}{3}\delta_{ij}\frac{\partial[u_k]}{\partial x_k} \ ; \ S_{ij} = \frac{1}{2}\left(\frac{\partial[u_i]}{\partial x_j} + \frac{\partial[u_j]}{\partial x_i}\right) \tag{5}$$

The k and ω budget equations are :

$$\frac{\partial\left\langle\rho\right\rangle[k]}{\partial t} = 0 = \underbrace{\left\langle\tau_{t,ij}\right\rangle\frac{\partial[u_i]}{\partial x_j}}_{\textbf{Production}} \underbrace{-\frac{\partial\left\langle\rho\right\rangle[k][u_j]}{\partial x_j}}_{\textbf{Advection}} \underbrace{+\frac{\partial}{\partial x_j}\left(\mu\frac{\partial[k]}{\partial x_j}\right)}_{\textbf{Molecular diffusion}} \underbrace{+\frac{\partial}{\partial x_j}\left(\frac{\mu_t}{\sigma_k}\frac{\partial[k]}{\partial x_j}\right)}_{\textbf{Turbulent transport \& pressure diffusion}} \underbrace{-c_k\left\langle\rho\right\rangle[k][\omega]}_{\textbf{Dissipation}} \tag{6}$$

$$\frac{\partial\left\langle\rho\right\rangle[\omega]}{\partial t} = 0 = \underbrace{c_{\omega 1}\frac{[\omega]}{[k]}\left\langle\tau_{t,ij}\right\rangle\frac{\partial[u_i]}{\partial x_j}}_{\textbf{Production}} \underbrace{-\frac{\partial\left\langle\rho\right\rangle[\omega][u_j]}{\partial x_j}}_{\textbf{Advection}} \underbrace{+\frac{\partial}{\partial x_j}\left(\left(\mu+\frac{\mu_t}{\sigma_\omega}\right)\frac{\partial[\omega]}{\partial x_j}\right)}_{\substack{\textbf{Turbulent transport,}\\ \textbf{pressure diffusion \&}\\ \textbf{molecular diffusion}}} \underbrace{-c_{\omega 2}\left\langle\rho\right\rangle[\omega]^2}_{\textbf{Dissipation}} \tag{7}$$

where $c_k = 0.09$, $c_{\omega 1} = 5/9$, $c_{\omega 2} = 3/40$, $\sigma_k = 2.0$ and $\sigma_\omega = 2.0$. Advection, molecular diffusion and turbulent transport terms are summed to form a transport term in the following analysis.

The QCR, proposed by Spalart [11], is a modification of Boussinesq constitutive relation in order to take into account the important effect of vorticity. The version we implemented is the modified one from Mani [22] in order to take into account the compressible part, given that *Turb'Flow* is a compressible solver:

$$\tau_{t,ij}^{QCR} = \tau_{t,ij} - c_{QCR}\left(O_{ik}\tau_{t,jk} + O_{jk}\tau_{t,ik}\right) \tag{8}$$

where $\boldsymbol{\tau_t}$ is the Boussinesq Reynolds stress tensor (Eq. (4)) and $\mathbf{O}$ is the normalised rotation tensor:

$$O_{ij} = \frac{\frac{\partial[u_i]}{\partial x_j} - \frac{\partial[u_j]}{\partial x_i}}{\sqrt{\frac{\partial[u_k]}{\partial x_l}\frac{\partial[u_k]}{\partial x_l}}} \text{ and } c_{QCR} = 0.3 \tag{9}$$

The k and ω equations remain the same as in the original model except that $\boldsymbol{\tau_t^{QCR}}$ is used instead of $\boldsymbol{\tau_t}$ in the production terms.

4 TOTAL PRESSURE LOSS

Total pressure losses are an important criterion for compressor efficiency. The total pressure loss coefficient Cp_t is defined as:

$$Cp_t = \frac{P_{t\infty} - P_t}{P_{t\infty} - P_{s\infty}} \tag{10}$$

where P_t is the local total pressure, $P_{t\infty}$ is the reference total pressure and $P_{s\infty}$ is the reference static pressure. For the RANS simulations, the reference pressures where taken 100mm upstream the leading edge, at a height of $h/4$.

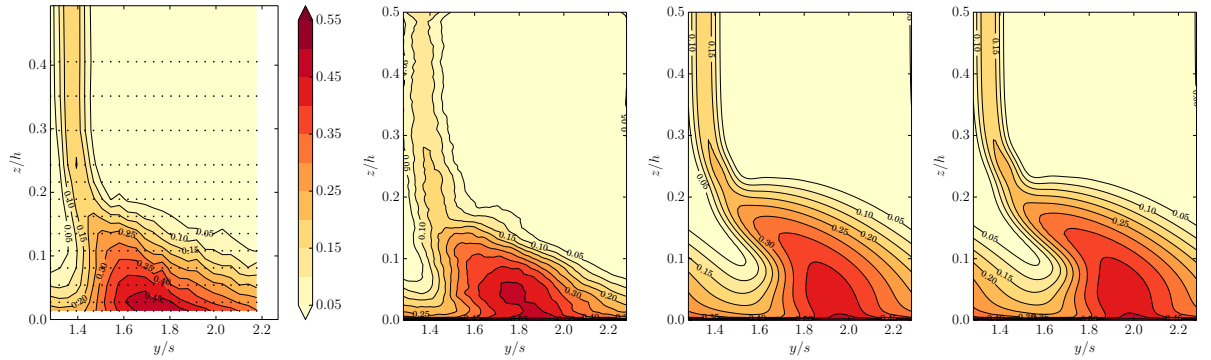

(a) Experiment (b) LES (c) RANS Wilcox 88 (d) RANS Wilcox 88 - QCR

Figure 3: Total pressure loss coefficient on the outlet plane at $1.907c_a$. (cf. Fig.1).

Experimental total pressure losses (Fig. 3a) and LES total pressure losses (Fig. 3b) are very similar. They both exhibit a triangular form for the corner separation wake, and display levels of pressure loss very similar. These results legitimate the usage of LES as a reference.

The RANS simulations over-predict the losses in each case. The use of a non-linear constitutive relation (QCR) yields almost no effect on the results (Fig. 3d) compared to the original Wilcox model (Fig. 3c). The wake of the corner separation is notably twisted in the RANS simulations. This could be an effect of the over-prediction of the size and intensity of the corner separation.

5 REYNOLDS STRESS TENSOR

The Reynolds stresses give a lot of information on the physics simulated. They are by nature a measure of the effect of the turbulence, thus they give a measure of the quality of the turbulence model for RANS simulations when compared with LES. Both normal stresses and shear stresses are affected by constitutive closure, so both have to be investigated against LES.

The Reynolds stresses are extracted at the trailing edge of the blade ($x = 1.0c_a$), on a rectangular surface covering the pitch. The plane position is given in Fig. 4.

In the following subsections, the Reynolds stresses are normalised by the product of a reference density ($\langle\overline{\rho_\infty}\rangle$ for LES, $\langle\rho_\infty\rangle$ for RANS simulations) times a reference velocity squared ($[\widetilde{u_\infty}]^2$ for LES, $[u_\infty]^2$ for RANS). The reference densities and velocities are taken 100mm upstream the leading edge, at a height of $h/4$.

5.1 Reynolds normal stresses

The Reynolds normal stresses ($\tau_{t,11}$, $\tau_{t,22}$ and $\tau_{t,33}$) are the main terms of the Reynolds stress tensor concerning intensity.

Figure 5 shows that both RANS simulations (Fig. 5b and 5c) over-predict the intensity of the first Reynolds normal stress compared to LES (Fig. 5a). The modification of the constitutive relation yields almost no effect in this case, $\tau_{t,11}$ and $\tau_{t,11}^{QCR}$ are similar.

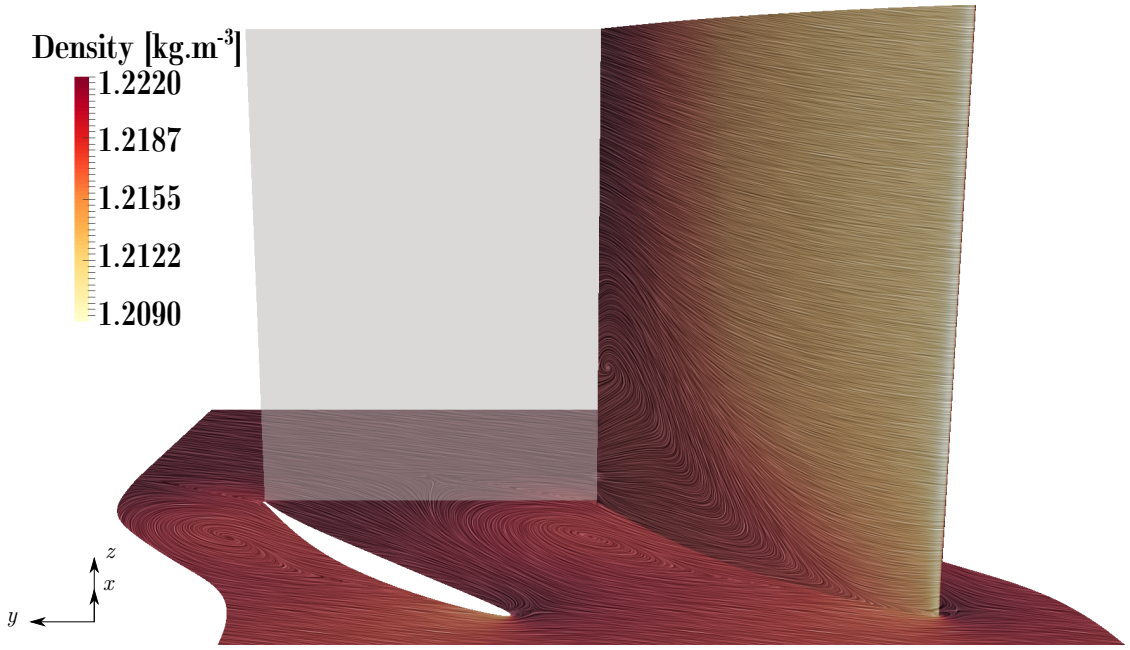

Figure 4: Extraction plane for the Reynolds stresses. Limiting streamlines are plotted for the RANS case, coloured by density.

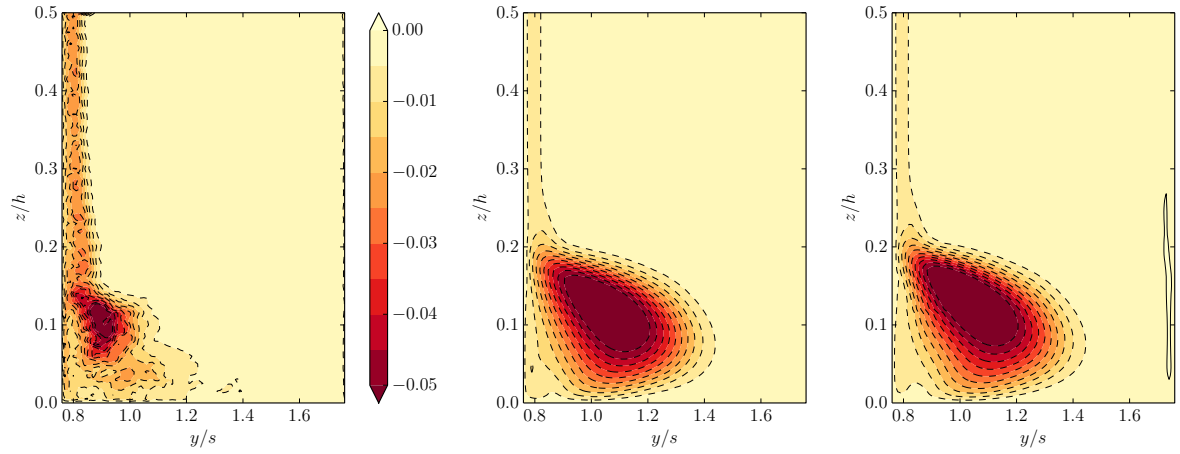

(a) LES (b) RANS Wilcox 88 (c) RANS Wilcox 88 - QCR

Figure 5: $\tau_{t,11}$ for LES (a), for RANS simulation with original Wilcox $k-\omega$ model (b) and $\tau_{t,11}^{QCR}$ for RANS simulation with QCR Wilcox $k-\omega$ model (c)

Figure 6 shows that the second Reynolds normal stress follows the same trend as the first one. The RANS simulations (Fig. 6b and 6c) still over-predict the intensity of $\tau_{t,22}$ compared to LES (Fig. 6a). However, the QCR has a more visible impact than previously. Compared to the Boussinesq closure, the QCR yields a lower minimum, more comparable with the minimum found by LES. However, both RANS simulations fail to represent the boundary-layer of the blade, visible in the LES for $y/s \simeq 0.8$.

Figure 7 shows that the third Reynolds normal stress follows the same trends as the first and second ones. The RANS simulations (Fig. 7b and 7c) over-predict the intensity of $\tau_{t,33}$ compared to LES (Fig. 7a). The impact of the QCR is noticeable on this term, compared with

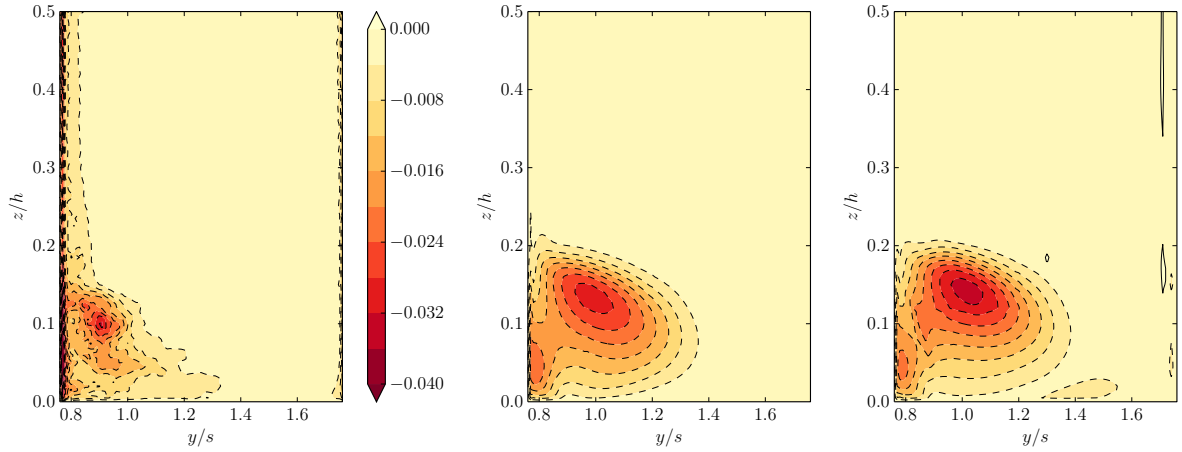

(a) LES (b) RANS Wilcox 88 (c) RANS Wilcox 88 - QCR

Figure 6: $\tau_{t,22}$ for LES (a), for RANS simulation with original Wilcox $k-\omega$ model (b) and $\tau_{t,22}^{QCR}$ for RANS simulation with QCR Wilcox $k-\omega$ model (c)

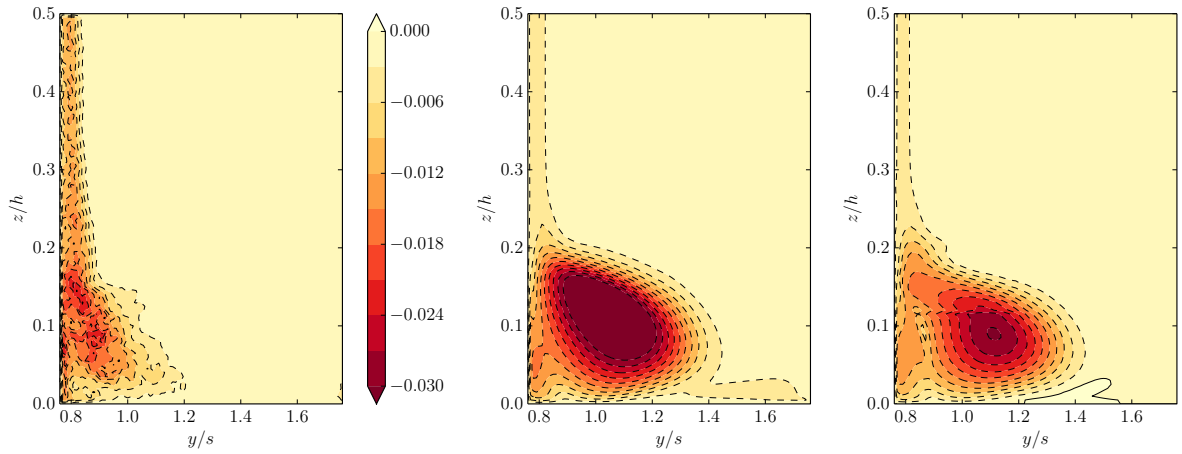

(a) LES (b) RANS Wilcox 88 (c) RANS Wilcox 88 - QCR

Figure 7: $\tau_{t,33}$ for LES (a), for RANS simulation with original Wilcox $k-\omega$ model (b) and $\tau_{t,33}^{QCR}$ for RANS simulation with QCR Wilcox $k-\omega$ model (c)

the original Wilcox model. It weakens the minimum of the Reynolds stress in the middle of the separation, but not enough to yield a value comparable with the LES.

5.2 Reynolds shear stresses

Reynolds shear stresses ($\tau_{t,12}$, $\tau_{t,13}$ and $\tau_{t,23}$) are of a lower intensity than the normal stresses.

Figure 8 shows that the first Reynolds shear stress is totally mispredicted by the RANS simulation with the original Wilcox turbulence model (Fig. 8b), compared to the LES (Fig. 8a). The minimum of this Reynolds shear stress should be close to the corner according to LES, and it should be more intense. The QCR modification improves the results by reducing the minimum and widening the area of negative stresses. It is still not enough to have the same levels, position, or the same physical behaviour as LES. Besides, both RANS simulations fail to predict the existence of stresses in the boundary-layer of the blade, visible in the LES for

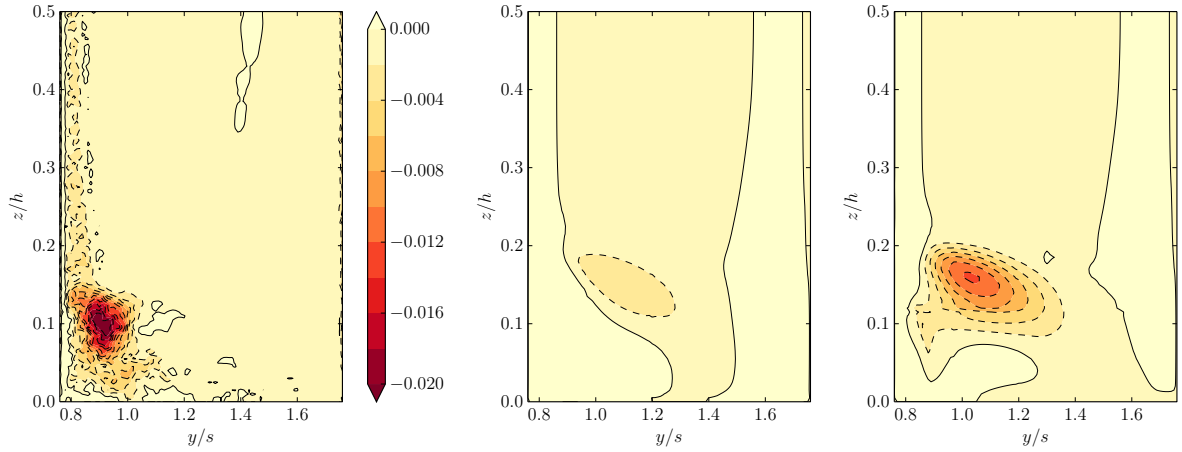

(a) LES (b) RANS Wilcox 88 (c) RANS Wilcox 88 - QCR

Figure 8: $\tau_{t,12}$ for LES (a), for RANS simulation with original Wilcox $k-\omega$ model (b) and $\tau_{t,12}^{QCR}$ for RANS simulation with QCR Wilcox $k-\omega$ model (c)

$y/s \simeq 0.8$.

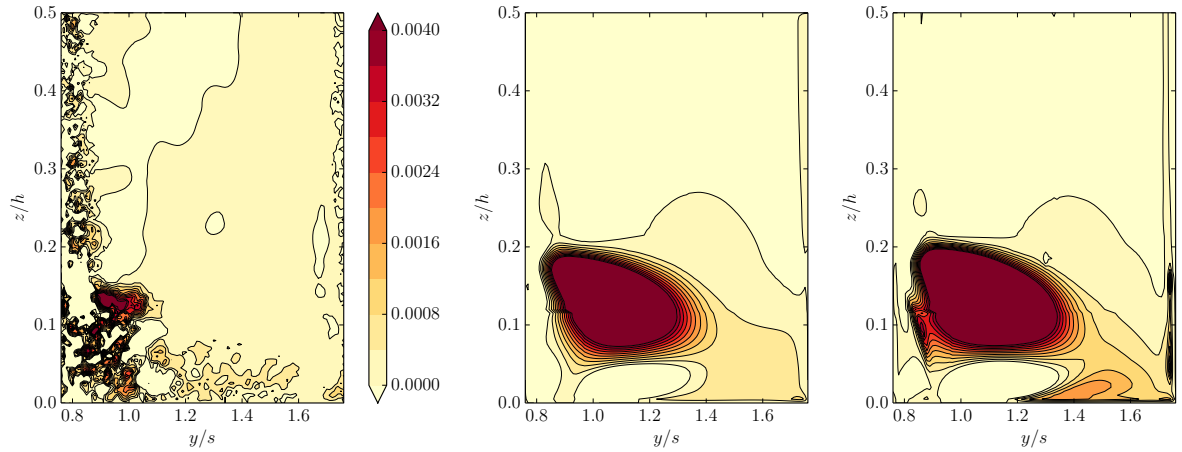

(a) LES (b) RANS Wilcox 88 (c) RANS Wilcox 88 - QCR

Figure 9: $\tau_{t,13}$ for LES (a), for RANS simulation with original Wilcox $k-\omega$ model (b) and $\tau_{t,13}^{QCR}$ for RANS simulation with QCR Wilcox $k-\omega$ model (c)

At the opposite, figure 9 shows that the second Reynolds shear stress is totally over-predicted by both RANS simulations (Fig. 9b and 9c) compared to LES (Fig. 9a). The area of the maximum plotted level is about ten times larger for RANS simulations than for LES, and QCR yields almost no differences from Boussinesq constitutive relation. The Wilcox model fails completely to predict this shear stress.

The third Reynolds shear stress follows the same trends as the second one, as shown in Fig. 10. The area of the maximum plotted level is about ten times larger for RANS simulations (Fig. 10b and 10c) than for LES (Fig. 10a), and QCR yields almost no differences with Boussinesq constitutive relation. Moreover, the stress maximum for both RANS simulations is further from the corner than for the LES.

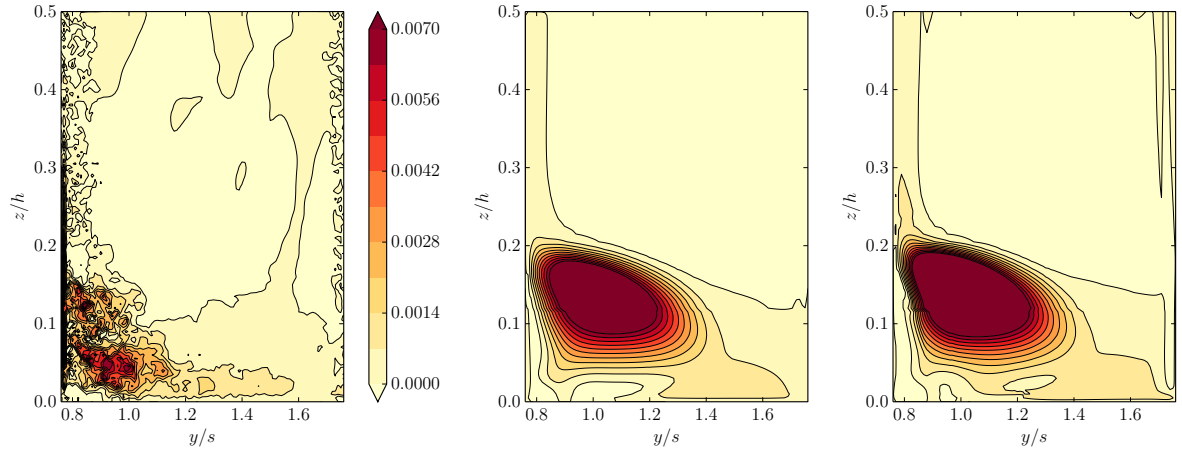

(a) LES (b) RANS Wilcox 88 (c) RANS Wilcox 88 - QCR

Figure 10: $\tau_{t,23}$ for LES (a), for RANS simulation with original Wilcox $k-\omega$ model (b) and $\tau_{t,23}^{QCR}$ for RANS simulation with QCR Wilcox $k-\omega$ model (c)

5.3 Synthesis

The comparisons between the RANS simulations and the LES have shown that the RANS simulations lead to a strong over-prediction of the Reynolds stresses compared to LES, except for $\tau_{t,12}$ whose amplitude is under-estimated. The Boussinesq constitutive relation and the QCR yield similar results in many cases, except for the Reynolds normal stress $\tau_{t,33}$ and the Reynolds shear stress $\tau_{t,12}$, where the influence of the QCR is beneficial. It is still not sufficient to correct the Wilcox $k-\omega$ model. The effect of turbulence is badly predicted in both RANS cases. The Reynolds stresses over-prediction can be put in parallel with the over-prediction of the total pressure loss. However, we do not know yet if the over-prediction of the separation leads to the over-prediction of the Reynolds stresses, or if the opposite occurs. The informations gathered do not allow to conclude yet.

6 TURBULENT KINETIC ENERGY BUDGET

The turbulent kinetic energy budget shows how the turbulent kinetic energy is created, transported and dissipated. For RANS, it measures the capacity of the turbulence model to represent correctly the physics of the local turbulent kinetic energy equilibrium.

The TKE budget is extracted at the trailing edge of the blade ($x = 1.0c_a$), on the same rectangular surface as for the extraction of the Reynolds stresses. The plane position is given in figure 4.

In the following subsections, the TKE budget terms are normalised by the ratio of the dynamic viscosity on the reference density squared ($\langle\overline{\rho_\infty}\rangle^2$ for LES, $\langle\rho_\infty\rangle^2$ for RANS simulations) times a reference velocity to the fourth power ($[\widetilde{u_\infty}]^4$ for LES, $[u_\infty]^4$ for RANS). The reference densities and velocities are taken 100mm upstream the leading edge, at a height of $h/4$.

In some of the LES figures, horizontal and vertical lines are visible. These do not represent any physical phenomenon, but are a consequence of the interpolation over many blocks of the computational domain for visualization.

6.1 Production

The production term represents the way turbulent kinetic energy is produced. Given its meaning and its expression, it is positive.

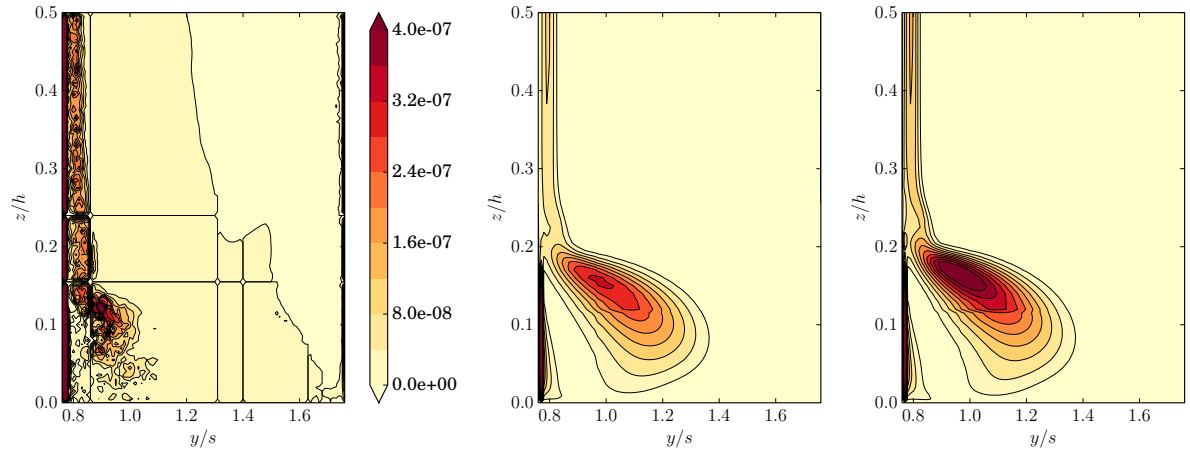

(a) LES (b) RANS Wilcox 88 (c) RANS Wilcox 88 - QCR

Figure 11: Turbulent kinetic energy production term.

The main area of production is in the separation, close to $z/h = 0.1$ (Fig. 11a). In the RANS simulations, all the Reynolds normal stresses are over-predicted. Consequently, the production term is over-predicted (Fig. 11b and 11c). The maximum is located upper in the span-wise direction for the RANS simulations than for the LES. The effect of the QCR is clearly visible, the intensity of the production term is more important and the area of high production is wider than for the Boussinesq constitutive relation.

6.2 Dissipation

The dissipation term of the TKE budget represents the damping of the turbulent kinetic energy.

For the LES, the major part of the dissipation occurs close to the blade, in the blade boundary-layer (Fig. 12a). A small amount of dissipation occurs also in the area of maximal production, on the corner-separation upper boundary. For the RANS simulations, similar levels of dissipation are observed in the blade boundary layers, but a strong dissipation is observed on the area of maximal production (Fig. 12b and 12c), in the corner separation. This is a known problem of RANS turbulence models, production and dissipation are superposed, with a small amount of transport (Ref. [23]). It is a non-physical behaviour. QCR slightly reduces the intensity of the dissipation term compared to Boussinesq constitutive relation.

6.3 Transport

The transport term is constructed to take into account all the transport effects. It can be positive (energy is added) or negative (energy is taken).

The LES transport term shows a physical behaviour (Fig. 13a). The TKE is taken from the area of production to be transported to the dissipative place, mostly close to the blade wall. The RANS models show no significant transport (Fig. 13b and 13c). The Wilcox turbulence model

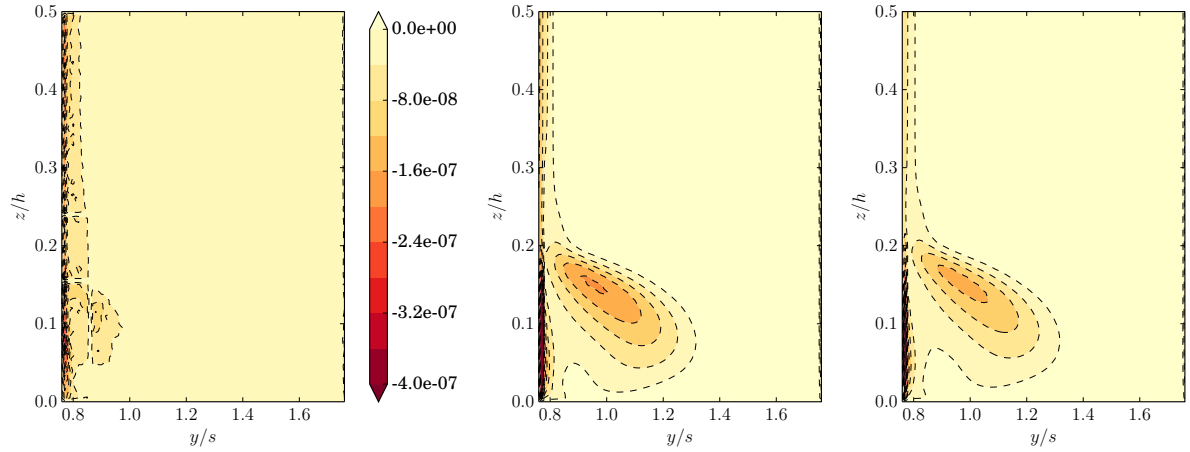

(a) LES (b) RANS Wilcox 88 (c) RANS Wilcox 88 - QCR

Figure 12: Turbulent kinetic energy dissipation term.

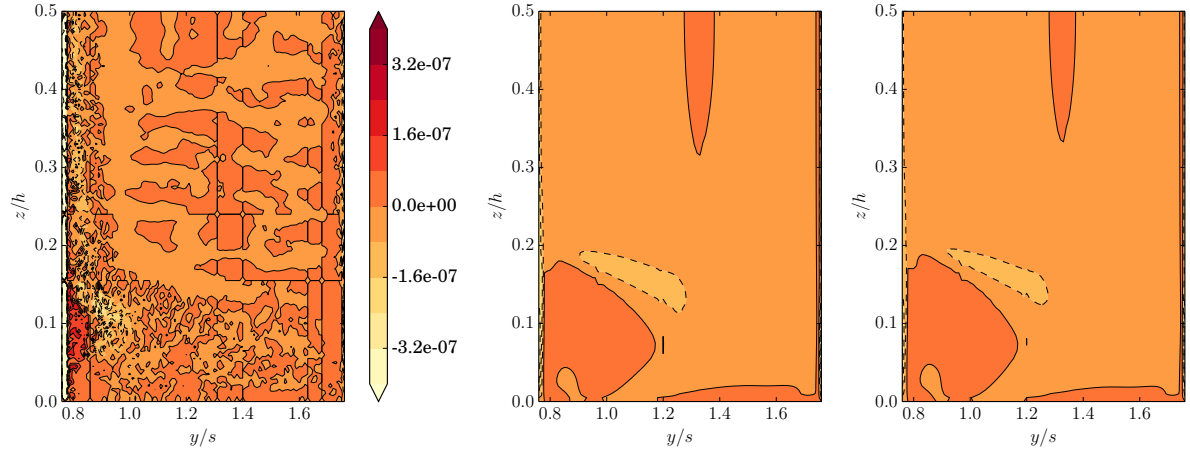

(a) LES (b) RANS Wilcox 88 (c) RANS Wilcox 88 - QCR

Figure 13: Turbulent kinetic energy transport term.

does not transport turbulent kinetic energy but produces and dissipates it in the same place. The QCR yields no significant effect on the transport term.

6.4 Numerical dissipation

The numerical dissipation is a non physical term accounting for the purely numerical effects on the TKE budget. For LES, it gives a measure of the quality of the simulation and budget extraction. For RANS, the modelled TKE equation is directly solved, so the residual should be driven to zero.

The LES numerical dissipation term is not negligible compared to the other budget terms (Fig. 14a) but remains moderate. It is negative and thus corresponds to dissipation. Its minimum is almost four times smaller in absolute value than extrema of production term or dissipation term in absolute value. The RANS simulations (Fig. 14b and 14c) show a numerical dissipation term not negligible, contrary to what was expected. This is not due to a default of the budget reconstruction, but to the use of a production term limiter. The original Wilcox

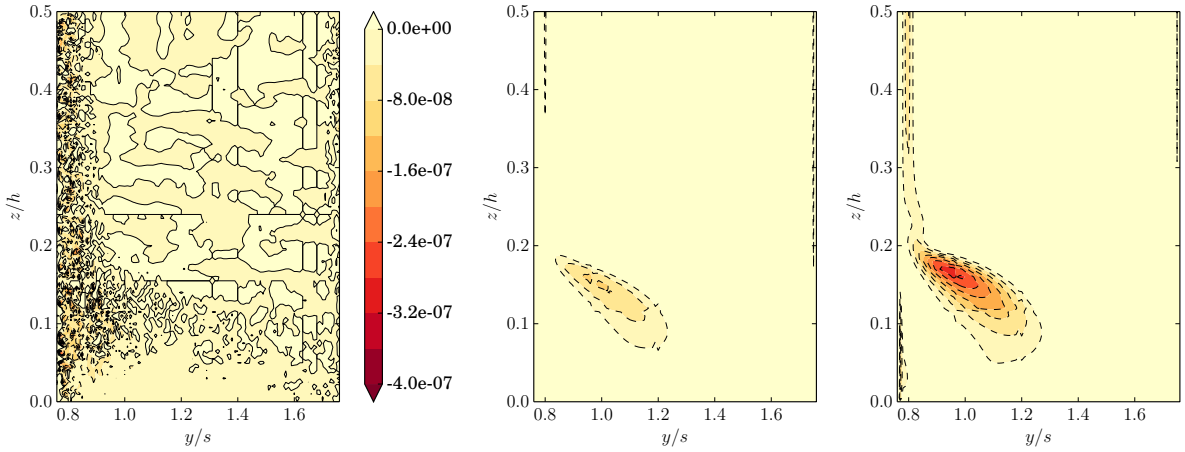

(a) LES (b) RANS Wilcox 88 (c) RANS Wilcox 88 - QCR

Figure 14: Turbulent kinetic energy numerical dissipation term.

$k-\omega$ model tends to over-predict k production at some points where anisotropy is important, such as leading-edge stagnation point or inside the corner separation. This default is inherent to two-equation models using Boussinesq constitutive relation [24]. To counterpart it, a strategy of k production limitation is implemented in *Turb'Flow*, in the form of a clipping of the production term [25]. Because the clipping is not implemented in the TKE budget extraction, the production term is more intense, and a non-null numerical dissipation term appears. The QCR closure introduces anisotropy in the Reynolds stresses. Far from decreasing the k production limiter effect, it increases it, by increasing the value of production and decreasing the value of dissipation (Fig. 14c).

7 CONCLUSIONS

- Large-eddy simulation yields good results according to the experiment, and was used as a reference to analyse RANS simulations.
- Large-eddy simulation yields results physically conclusive for the fine behaviour of the turbulence, for Reynolds stresses and turbulent kinetic energy budget.
- The RANS simulations analysed failed to represent correctly the Reynolds normal and shear stresses. An important over-prediction or under-prediction was observed.
- The QCR closure model yields some modifications, mainly on two terms, $\tau_{t,33}$ and $\tau_{t,12}$, but not significant enough to have results comparable to LES.
- The RANS simulations fail to represent the turbulent kinetic energy budget. The main failure comes from the impossibility to represent correctly the transport of turbulent kinetic energy.
- The QCR tends to activate more the k-production limiter in the corner separation than the Boussinesq closure.

ACKNOWLEDGEMENTS

This study was supported by the Franco-Chinese project VortexFlowCFD, funded by the French National Research and Technology Agency (ANRT) and the SNECMA industry.

The simulations were performed using HPC resources from GENCI-CINES (Grant 2015-2a5039).

REFERENCES

[1] F. Gao, W. Ma, G. Zambonini, J. Boudet, X. Ottavy, L. Lu, and L. Shao, "Large-eddy simulation of 3-D corner separation in a linear compressor cascade," *Physics of Fluids*, vol. 27, p. 085105, Aug. 2015.

[2] W. Ma, X. Ottavy, L. Lu, F. Leboeuf, and F. Gao, "Experimental Study of Corner Stall in a Linear Compressor Cascade," *Chinese Journal of Aeronautics*, vol. 24, pp. 235–242, June 2011.

[3] A. M. Yocum and W. F. O'Brien, "Separated Flow in a Low-Speed Two-Dimensional Cascade: Part I-Flow Visualization and Time-Mean Velocity Measurements," *Journal of Turbomachinery*, vol. 115, pp. 409–420, July 1993.

[4] A. M. Yocum and W. F. O'Brien, "Separated Flow in a Low-Speed Two-Dimensional Cascade: Part II-Cascade Performance," *Journal of Turbomachinery*, vol. 115, pp. 421–434, July 1993.

[5] W. Ma, X. Ottavy, L. Lu, and F. Leboeuf, "Intermittent corner separation in a linear compressor cascade," *Experiments in Fluids*, vol. 54, pp. 1–17, June 2013.

[6] C. Hah and J. Loellbach, "Development of hub corner stall and its influence on the performance of axial compressor blade rows," *Journal of turbomachinery*, vol. 121, no. 1, pp. 67–77, 1999.

[7] Y. Liu, L. Lu, L. Fang, and F. Gao, "Modification of Spalart–Allmaras model with consideration of turbulence energy backscatter using velocity helicity," *Physics Letters A*, vol. 375, pp. 2377–2381, June 2011.

[8] Y. Liu, H. Yan, L. Fang, L. Lu, Q. Li, and L. Shao, "Modified k-ω model using kinematic vorticity for corner separation in compressor cascades," *Science China Technological Sciences*, Jan. 2016.

[9] F. Gao, W. Ma, J. Sun, J. Boudet, X. Ottavy, Y. Liu, L. Lu, and L. Shao, "Parameter study on numerical simulation of corner separation in lmfa-naca65 linear compressor cascade," Submitted to *Chinese Journal of Aeronautics*.

[10] M. Bordji, F. Gand, S. Deck, and V. Brunet, "Investigation of a Nonlinear Reynolds-Averaged Navier–Stokes Closure for Corner Flows," *AIAA Journal*, pp. 1–13, Sept. 2015.

[11] P. R. Spalart, "Strategies for turbulence modelling and simulations," *International Journal of Heat and Fluid Flow*, vol. 21, no. 3, pp. 252–263, 2000.

[12] J. Boudet, A. Cahuzac, P. Kausche, and M. C. Jacob, "Zonal Large-Eddy Simulation of a Fan Tip-Clearance Flow, With Evidence of Vortex Wandering," *Journal of Turbomachinery*, vol. 137, p. 061001, June 2015.

[13] F. Gao, G. Zambonini, J. Boudet, X. Ottavy, L. Lu, and L. Shao, "Unsteady behavior of corner separation in a compressor cascade: Large eddy simulation and experimental study," *Proceedings of the Institution of Mechanical Engineers, Part A: Journal of Power and Energy*, vol. 229, pp. 508–519, Aug. 2015.

[14] G. Zambonini and X. Ottavy, "Unsteady Pressure Investigations of Corner Separated Flow in a Linear Compressor Cascade," p. V02CT44A002, ASME, June 2015.

[15] J. Boudet, J. Caro, L. Shao, and E. Lévêque, "Numerical studies towards practical large-eddy simulation," *Journal of Thermal Science*, vol. 16, pp. 328–336, Nov. 2007.

[16] A. Jameson, W. Schmidt, E. Turkel, and others, "Numerical solutions of the Euler equations by finite volume methods using Runge-Kutta time-stepping schemes," *AIAA paper*, vol. 1259, p. 1981, 1981.

[17] J. Boudet, J. F. Monier, and F. Gao, "Implementation of a roughness element to trip transition in large-eddy simulation," *Journal of Thermal Science*, vol. 24, pp. 30–36, Feb. 2015.

[18] E. Lévêque, F. Toschi, L. Shao, and J.-P. Bertoglio, "Shear-improved Smagorinsky model for large-eddy simulation of wall-bounded turbulent flows," *Journal of Fluid Mechanics*, vol. 570, p. 491, Jan. 2007.

[19] A. Cahuzac, J. Boudet, P. Borgnat, and E. Lévêque, "Smoothing algorithms for mean-flow extraction in large-eddy simulation of complex turbulent flows," *Physics of Fluids*, vol. 22, no. 12, p. 125104, 2010.

[20] F. Gao, *Advanced numerical simulation of corner separation in a linear compressor cascade*. PhD Thesis, Ecole Centrale de Lyon, Ecully, 2014.

[21] D. Wilcox, C., "Reassessment of the scale-determining equation for advanced turbulence models," *AIAA Journal*, vol. 26, no. 11, pp. 1299 – 1310, 1988.

[22] M. Mani, D. Babcock, C. Winkler, and P. Spalart, "Predictions of a Supersonic Turbulent Flow in a Square Duct," American Institute of Aeronautics and Astronautics, Jan. 2013.

[23] D. C. Wilcox, *Turbulence Modeling for CFD*. D C W Industries, 3rd edition ed.

[24] W. C. STRAHLE, "Stagnation point flows with freestream turbulence - The matching condition," *AIAA Journal*, vol. 23, pp. 1822–1824, Nov. 1985.

[25] F. R. Menter, "Two-equation eddy-viscosity turbulence models for engineering applications," *AIAA Journal*, vol. 32, pp. 1598–1605, Aug. 1994.